Journal of Advanced Ceramics
2020, **9**(2): 204–209
https://doi.org/10.1007/s40145-020-0360-2

ISSN 2226-4108
CN 10-1154/TQ

Research Article

Determination of polarization states in $(K,Na)NbO_3$ lead-free piezoelectric crystal

Mao-Hua ZHANG[a], Chengpeng HU[b,*], Zhen ZHOU[a], Hao TIAN[b], Hao-Cheng THONG[a], Yi Xuan LIU[a], Xing-Yu XU[a], Xiao-Qing XI[a], Jing-Feng LI[a], Ke WANG[a,*]

[a]*State Key Laboratory of New Ceramics and Fine Processing*, *School of Materials Science and Engineering*, *Tsinghua University*, *Beijing 100084*, *China*
[b]*Department of Physics*, *Harbin Institute of Technology*, *Harbin 150001*, *China*

Received: October 15, 2019; Revised: January 6, 2020; Accepted: January 6, 2020

Abstract: Polarization switching in lead-free $(K_{0.40}Na_{0.60})NbO_3$ (KNN) single crystals was studied by switching spectroscopy piezoresponse force microscopy (SS-PFM). Acquisition of multiple hysteresis loops on a closely spaced square grid enables polarization switching parameters to be mapped in real space. Piezoresponse amplitude and phase hysteresis loops show collective symmetric/asymmetric characteristics, affording information regarding the switching behavior of different domains. As such, the out-of-plane polarization states of the domains, including amplitudes and phases can be determined. Our results could contribute to a further understanding of the relationships between polarization switching and polarization vectors at the nanoscale, and provide a feasible method to correlate the polarization hysteresis loops in a domain under an electric field with the polarization vector states.

Keywords: piezoelectrics; lead-free; $(K_{0.40}Na_{0.60})NbO_3$ (KNN); switching spectroscopy piezoresponse force microscopy (SS-PFM); ferroelectric domain

1 Introduction

Spontaneous polarization that can be switched by an electric field from one direction to another is the defining feature of ferroelectric crystals, which has long provided the functional foundation for various applications including modern non-volatile memories [1,2], sensor and actuators [3,4], and infrared imaging systems [5]. Domains are coherent regions with uniform polarization directions and significantly contribute to the electromechanical properties of ferroelectrics [6–9]. Characterization of the responses of domains to external electric stimuli is necessary for a better understanding of local electromechanical functionalities and enables a correlation between microscopic order and macroscopic properties, which is significant to develop high-performance next-generation ferroelectrics.

Piezoresponse force microscopy (PFM) has emerged as a powerful tool to probe local piezoelectric and ferroelectric properties of ferroelectrics at the nanoscale [10–17]. In a typical PFM setup, an AC electrical voltage is applied to the sample surface with a conductive cantilever tip, which induces a structural change as a result of piezoelectricity and in turn, the

* Corresponding authors.
E-mail: C. Hu, huchengpeng1988@163.com;
K. Wang, wang-ke@tsinghua.edu.cn

deflection of the cantilever. This provides local deformation responses that can be interpreted in terms of the piezoelectric properties. The invention of PFM has enabled sub-10 nm resolution imaging of domain structures and local polarization control [18,19].

Polarization vectors consisting of polarization directions and magnitudes are intrinsic properties of domains, which respond to electric stimuli and can be probed by PFM. Characterization of local polarization vectors is of significance to better understand the macroscopic properties of the piezoelectrics. Polarization orientations can be identified by poling experiments, i.e., applying a positive or negative pulsed bias to see how phase contrast changes or conducting switching hysteresis loops. However, only polarization direction rather than magnitude can be identified during poling experiments. And the response of domains to electric stimuli that encoded in the switching hysteresis loops is also missing.

Here, we report an approach to determine the polarization vector states based on mapping of switching behavior obtained using switching spectroscopy piezoresponse force microscopy (SS-PFM). This recognized technique enables quantitative characterization of the local switching behavior of ferroelectrics and a detailed description is given by Refs. [20–22]. In this study, polarization vectors are qualitatively determined based on hysteresis loops (amplitude and symmetry) of the mapping results. Considering the shapes of hysteresis loops are subjected to other contributing mechanisms including electrostatic charge, mechanical clamping, and substrate, high quality lead-free potassium sodium niobate $(K_{0.40}Na_{0.60})NbO_3$ (KNN) single crystals are adopted in this study to guarantee hysteresis loops are mainly contributed by the polarization direction and magnitude of the domains. The crystals in our study offer a playground to demonstrate our approach, which is impractical in polycrystalline piezoelectrics where polarization states are randomly distributed and unknown. Also, lead-free materials are chosen with the consideration of environmental concerns over lead-based piezoelectrics [23–26].

2 Experimental

The preparation process of the $[001]_c$-oriented KNN single crystal was described by Ref. [27]. The crystal is in orthorhombic structure and the domain wall shown in Fig. 1(b) orients along $[001]_c$. The crystal was polished with diamond paste down to 0.25 μm particle size and the thickness of the crystal is 0.4 mm. The crystal was annealed at 400 ℃ for 2 h afterwards. PFM and SS-PFM were implemented on a commercial Cypher AFM (Asylum Research, Santa Barbara, CA, USA), using Pt and Ir coated cantilever (NanoWorld EFM, force constant 2.8 N/m, resonance frequency 75 kHz). Domain structures were acquired using vertical dual amplitude resonance tracking (DART) mode, where an AC voltage of 0.5 V at a frequency of 300 kHz was applied to the cantilever. Local ferroelectric switching behavior was mapped by SS-PFM, where a TriangleSquare function with a maximum value of 20 V at 0.2 Hz, was applied to facilitate ferroelectric domain switching. Phase of the drive wave is 1 (from 0 to 1) and the period of one square wave pulse is 0.10. A modulated AC voltage of 0.5 V was simultaneously superimposed to acquire data. Contact resonance peaks show symmetric behavior and the piezoresponse hysteresis loops obtained using DART mode were then corrected via simple harmonic oscillator (SHO) model [12,28]. Only off-field hysteresis loops were analyzed

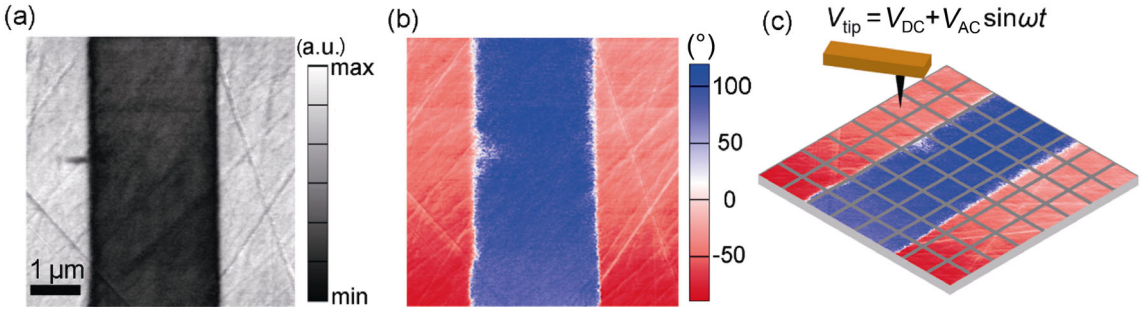

Fig. 1 PFM imaging and a schematic of tip movement during SS-PFM mapping. (a) Piezoresponse amplitude and (b) phase contrast images of the KNN single crystals. (c) In SS-PFM, local hysteresis loops are collected using a waveform at each point on 25 × 25 mesh. Detailed description of SS-PFM was previously reported by Ref. [20]. The domain wall shown in Fig. 1(b) orients along $[001]_c$.

and plotted in this study. Mapping results were output using the FMapCalcPFMoff function under the Analyze tab in the Master Force Panel, Igor Program.

3 Results and discussion

PFM imaging of the KNN single crystals is shown in Figs. 1(a) and 1(b), where regular stripe domains are observed. A low piezoresponse is observed for the middle domain while a high piezoresponse is found for the two side domains on the left and right sides of the image. A 180° phase contrast indicates the directions of the out-of-plane (OP) polarization components for the middle and side domains are opposite. However, the exact directions of the OP polarization components, i.e., whether the components are upwards or downwards, cannot be unambiguously determined here. Hence, local ferroelectric switching responses are collected using SS-PFM at each point on 25 × 25 mesh, yielding a total of 625 hysteresis loops, which enable a comprehensive analysis of collective domain switching behavior.

Typical results of all the 625 hysteresis loops are firstly analyzed to clarify different switching behaviors in different domains. Maps of switching parameters are subsequently output to demonstrate the collective behaviors. Piezoresponse amplitude curves for the middle and side domains are shown in Figs. 2(a) and 2(c), which are the average results of 100 points and are representative of all the 625 points. Asymmetric butterfly curves are observed for both the middle and side domains but are different in shapes and degrees of asymmetry. The maximum amplitudes on the positive half axis are lower for the middle domain while higher for the side domains, when compared with those on the negative half axis. A higher degree of asymmetry is noticed for the side domains, where the amplitude differences between the positive and negative half axes are more obvious. Piezoresponse phase images for the middle and side domains are shown in Figs. 2(b) and 2(d), where positive coercive bias V_c^+ and negative coercive bias V_c^- are defined. Note that V_c^+ and V_c^- are not specific values but correspond to voltage ranges where error bars maximize in hysteresis phase loops. They can also refer to the voltages where drastic variation in phase initiates and a new domain nucleates [20,29], which are different from the concepts in polarization–electric field (P–E) loops for bulk piezoelectrics. For the middle domain, V_c^+ is slightly larger than V_c^- in absolute values, resulting in a shift of loops towards the positive axis direction. For the side domains, V_c^+ is smaller than V_c^- in absolute values, and a shift towards the negative axis direction is developed.

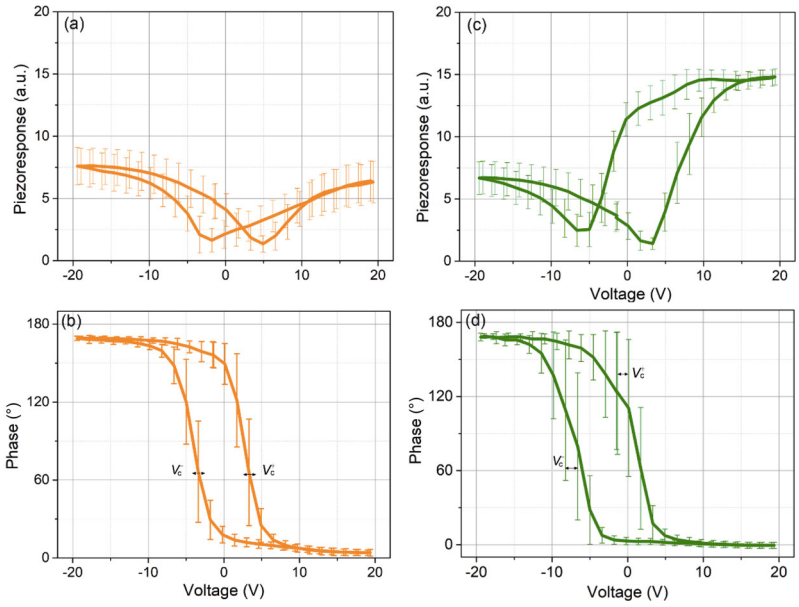

Fig. 2 Comparisons of PFM hysteresis loops between the (a, b) middle and (c, d) side domains. Hysteresis loops shown are the average results of 100 points in the respective domains. Positive bias V_c^+ and negative bias V_c^- are not specific values but correspond to voltage ranges where error bars maximize in hysteresis phase loops. V_c^+ and V_c^- correspond to the voltages where drastic variation in phase happens.

Collective domain switching behaviors of different regions within the middle and side domains can be revealed by SS-PFM mapping, which has statistical significance. Maps of positive and negative coercive biases are shown in Figs. 3(b) and 3(c), respectively. For the middle domain, the values of V_c^+ and V_c^- are around +4 V and (−4)−(−2) V, respectively. For the side domains, V_c^- and V_c^- are quite different in values, which are around −2 V and (−8)−(−6) V, respectively. The difference between positive and negative coercive biases accounts for the asymmetric features of hysteresis curves, as shown in Fig. 2. A map of imprint $(V_c^- + V_c^-)/2$ is shown in Fig. 3(d), which can be used to estimate the degree of asymmetry of hysteresis curves. Note that there is a region in the bottom part of the middle domains showing inconsistent coercive bias results. This is due to the shapes of hysteresis loops from this region are not well defined (Figs. S1 and S2 in the Electronic Supplementary Material). And the FMapCalcPFMoff function we used in the Igor program cannot correctly recognize bias values from poorly defined hysteresis loops, leading to inconsistent results. Hence, hysteresis results shown in Fig. 2 do not include results from this region. The origins of these results are unclear. Considering there are only 30 points showing poorly shaped hysteresis loops and the remaining more than 600 points showing consistent switching behavior, the results from this region do not preclude the determination of the collective switching behavior of the domains.

Based on the above results, the OP polarization vector states can be qualitatively determined based on the amplitudes and symmetry of the hysteresis loops. If there is no OP polarization component within a domain, hysteresis curves should be symmetric, i.e., no shift along either positive or negative half axis direction. Once there is an OP spontaneous polarization component, there is a strong unwillingness of the polarization switching along the opposite direction of the spontaneous polarization and in turn, asymmetric curves will be developed, as observed in Fig. 2.

The directions of OP spontaneous polarization components can be determined from the shifts of hysteresis loops. For the middle domain, hysteresis loops shift along the positive half axis direction, indicating that it is easier to induce polarization component to orient upwards under an upwards electric field. Thus, OP spontaneous polarization component is upwards for the middle domain, as shown in Fig. 4(a). For the side domains, in contrast, the shifts of hysteresis loops along the negative half axis direction indicate a downwards OP spontaneous polarization component (Fig. 4(a)).

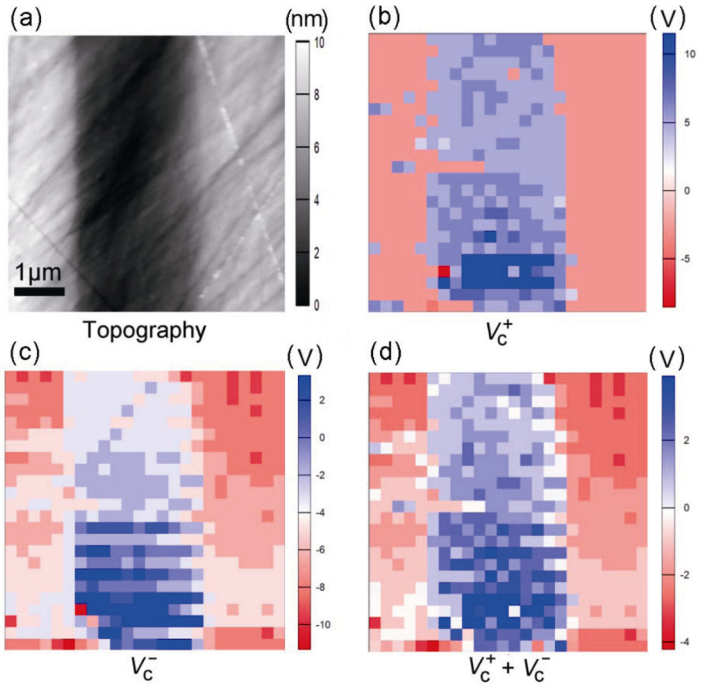

Fig. 3 (a) Surface topography and maps of switching parameters of the KNN single crystals obtained using SS-PFM: (b) positive bias V_c^+, (c) negative bias V_c^-, and (d) imprint = $(V_c^+ + V_c^-)/2$.

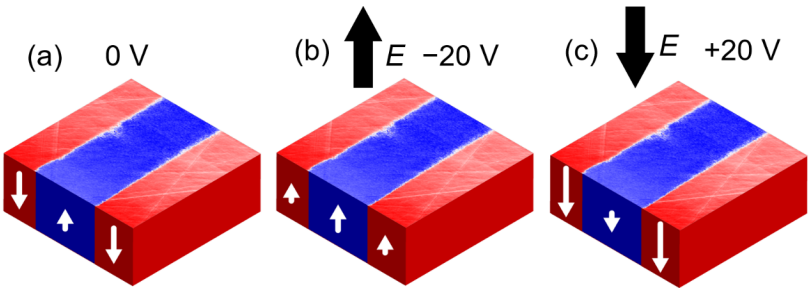

Fig. 4 Schematics of OP polarization components of the KNN single crystals in the as-grown state (Figs. 1(a) and 1(b)) and under electric fields. (a) As-grown state of the crystals, showing the directions and magnitudes of the spontaneous OP polarization components within the middle and side domains. (b) Under the maximum negative voltage, OP polarization components of the middle and side domains are aligned along the electric-field direction (upwards) but with different magnitudes (smaller in side domains). (c) Under the maximum positive voltage, OP polarization vector components of the middle and side domains are aligned along the electric-field direction (downwards) but with different magnitudes (much larger in side domains). The lengths of the arrows represent the magnitudes of polarization components, corresponding to the amplitudes of hysteresis curves in Fig. 2.

The amplitudes of OP spontaneous polarization components can be estimated from the amplitudes of hysteresis loops. For the middle domain, the difference in amplitudes on the positive and negative axes is limited, indicating a low degree of anisotropy. This can be explained by the presence of a small magnitude of OP spontaneous polarization component for the middle domain. Under an upwards electric field (−20 V), the amplitude of the middle domain is slightly larger because electric field and spontaneous polarization are in the same direction (Fig. 4(b)). Under a downwards electric field (+20 V), the amplitude of the middle domain is smaller as a result of the opposite direction of polarization to that of electric field (Fig. 4(c)). For the side domains, the amplitude on the positive axis is much higher than that on the negative axis. This is due to the presence of a large magnitude of OP spontaneous polarization component. Similarly, amplitude will be increased or decreased when the direction of OP spontaneous polarization component is in the same or opposite direction to that of electric field. Based on the above analyses, schematics of OP polarization component for the KNN single crystals under different states are shown in Fig. 4.

4 Conclusions

To summarize, SS-PFM mapping was performed for the KNN single crystals and a number of 625 hysteresis loops were obtained. The collective asymmetric features of the loops are due to different polarization directions of the domains. Based on the collective polarization switching behavior, the initial OP polarization states can be determined. Our results reveal the relationships between polarization switching and polarization vectors.

Acknowledgements

This work was supported by Science Challenge Project (No. TZ2018003) and National Natural Science Foundation of China (Grant Nos. 51822206 and 5171101344).

Electronic Supplementary Material

Supplementary material is available in the online version of this article at https://doi.org/10.1007/s40145-020-0360-2.

References

[1] Chanthbouala A, Crassous A, Garcia V, *et al*. Solid-state memories based on ferroelectric tunnel junctions. *Nature Nanotech* 2012, **7**: 101–104.

[2] Hoffman J, Pan X, Reiner JW, *et al*. Ferroelectric field effect transistors for memory applications. *Adv Mater* 2010, **22**: 2957–2961.

[3] Muralt P. Ferroelectric thin films for micro-sensors and actuators: A review. *J Micromech Microeng* 2000, **10**: 136–146.

[4] Rödel J, Webber KG, Dittmer R, *et al*. Transferring lead-free piezoelectric ceramics into application. *J Eur Ceram Soc* 2015, **35**: 1659–1681.

[5] Lang SB. Pyroelectricity: from ancient curiosity to modern imaging tool. *Phys Today* 2005, **58**: 31–36.

[6] Damjanovic D. Stress and frequency dependence of the direct piezoelectric effect in ferroelectric ceramics. *J Appl Phys* 1997, **82**: 1788–1797.

[7] Damjanovic D. Contributions to the piezoelectric effect in ferroelectric single crystals and ceramics. *J Am Ceram Soc* 2005, **88**: 2663–2676.

[8] Porokhonskyy V, Damjanovic D. Domain wall contributions in Pb(Zr,Ti)O_3 ceramics at morphotropic phase boundary: A study of dielectric dispersion. *Appl Phys Lett* 2010, **96**: 242902.

[9] Zhang QM, Wang H, Kim N, *et al*. Direct evaluation of domain-wall and intrinsic contributions to the dielectric and piezoelectric response and their temperature dependence on lead zirconate-titanate ceramics. *J Appl Phys* 1994, **75**: 454–459.

[10] Li JY, Li JF, Yu Q, *et al*. Strain-based scanning probe microscopies for functional materials, biological structures, and electrochemical systems. *J Materiomics* 2015, **1**: 3–21.

[11] Li JY, Rogan RC, Üstündag E, *et al*. Domain switching in polycrystalline ferroelectric ceramics. *Nat Mater* 2005, **4**: 776–781.

[12] Xie SH, Gannepalli A, Chen QN, *et al*. High resolution quantitative piezoresponse force microscopy of $BiFeO_3$nanofibers with dramatically enhanced sensitivity. *Nanoscale* 2012, **4**: 408–413.

[13] Balke N, Bdikin I, Kalinin SV, *et al*. Electromechanical imaging and spectroscopy of ferroelectric and piezoelectric materials: State of the art and prospects for the future. *J Am Ceram Soc* 2009, **92**: 1629–1647.

[14] Hong S, Woo J, Shin H, *et al*. Principle of ferroelectric domain imaging using atomic force microscope. *J Appl Phys* 2001, **89**: 1377–1386.

[15] Hong S, Ecabart B, Colla EL, *et al*. Three-dimensional ferroelectric domain imaging of bulk Pb(Zr, Ti)O_3 by atomic force microscopy. *Appl Phys Lett* 2004, **84**: 2382–2384.

[16] Colla EL, Hong S, Taylor DV, *et al*. Direct observation of region by region suppression of the switchable polarization (fatigue) in Pb(Zr, Ti)O_3 thin film capacitors with Pt electrodes. *Appl Phys Lett* 1998, **72**: 2763–2765..

[17] Huey BD. AFM and acoustics: Fast, quantitative nanomechanical mapping. *Annu Rev Mater Res* 2007, **37**: 351–385.

[18] Alexe M, Gruverman A. *Nanoscale Characterisation of Ferroelectric Materials*. Berlin, Heidelberg: Springer Berlin Heidelberg, 2004.

[19] Hong S. *Nanoscale Phenomena in Ferroelectric Thin Films.* Boston, MA: Springer US, 2004.

[20] Jesse S, Baddorf AP, Kalinin SV. Switching spectroscopy piezoresponse force microscopy of ferroelectric materials. *Appl Phys Lett* 2006, **88**: 062908.

[21] Jesse S, Lee HN, Kalinin SV. Quantitative mapping of switching behavior in piezoresponse force microscopy. *Rev Sci Instruments* 2006, **77**: 073702.

[22] Rodriguez BJ, Jesse S, Baddorf AP, *et al*. Spatially resolved mapping of ferroelectric switching behavior in self-assembled multiferroic nanostructures: Strain, size, and interface effects. *Nanotechnology* 2007, **18**: 405701.

[23] Rödel J, Jo W, Seifert KTP, *et al*. Perspective on the development of lead-free piezoceramics. *J Am Ceram Soc* 2009, **92**: 1153–1177.

[24] Koruza J, Bell AJ, Frömling T, *et al*. Requirements for the transfer of lead-free piezoceramics into application. *J Materiomics* 2018, **4**: 13–26.

[25] Wu JG, Xiao DQ, Zhu JG. Potassium–sodium niobate lead-free piezoelectric materials: Past, present, and future of phase boundaries. *Chem Rev* 2015, **115**: 2559–2595.

[26] Wang K, Malič B, Wu JG. Shifting the phase boundary: Potassium sodium niobate derivates. *MRS Bull* 2018, **43**: 607–611.

[27] Hu CP, Tian H, Meng XD, *et al*. High-quality $K_{0.47}Na_{0.53}NbO_3$ single crystal toward high performance transducer. *RSC Adv* 2017, **7**: 7003–7007.

[28] Gannepalli A, Yablon DG, Tsou AH, *et al*. Mapping nanoscale elasticity and dissipation using dual frequency contact resonance AFM. *Nanotechnology* 2011, **22**: 355705.

[29] Kalinin SV, Rodriguez BJ, Jesse S, *et al*. Local bias-induced phase transitions. *Mater Today* 2008, **11**: 16–27.